Chiral selectivity of improper ferroelectricity in single-wall $PbTiO_3$ nanotubes

Jie Wang,[1,2,*] Tao Xu,[1] Takahiro Shimada,[2] Xiaoyuan Wang,[3] Tong-Yi Zhang,[4] and Takayuki Kitamura[2]

[1]*Department of Engineering Mechanics, School of Aeronautics and Astronautics, Zhejiang University, Hangzhou 310027, China*

[2]*Department of Mechanical Engineering and Science, Kyoto University, Nishikyo-ku, Kyoto 615-8540, Japan*

[3]*Institute of Systems Engineering, China Academy of Engineering Physics, Postbox 919-401, Mianyang 621900, China*

[4]*Department of Mechanical and Aerospace Engineering, The Hong Kong University of Science and Technology, Clear Water Bay, Hong Kong, China*

(Received 1 December 2013; revised manuscript received 19 February 2014; published 2 April 2014)

Full density functional theory calculations successfully demonstrate that a remarkable spontaneous polarization can stably exist in extremely thin $PbTiO_3$ single-wall nanotubes (PTO-SWNTs) folded from (110) nanosheets with a specific chirality of (m, 0), whereas ferroelectricity is absent from nanotubes with other chiralities and from the unfolded thin films. In other words, there is chiral selectivity of ferroelectricity. The chirality of the ferroelectric (FE) nanotubes plays a variety of significant roles in (i) the stabilization of a low-energy single-wall tubular structure, (ii) the emergence of antiferrodistortive (AFD) distortion hidden in the $PbTiO_3$ bulk, and (iii) the strong coupling between FE and emergent AFD distortions. The direct FE-AFD coupling stabilizes the remarkable FE distortion in these ultrathin nanotubes through tilting of oxygen octahedra, suggesting improper ferroelectricity. The existence of a large spontaneous polarization suggests that PTO-SWNTs hold promise for applications in advanced sensors and nanoscale energy-harvesting devices.

DOI: 10.1103/PhysRevB.89.144102 PACS number(s): 77.80.−e, 31.15.E−, 77.22.Ej

I. INTRODUCTION

Ferroelectric (FE) nanotubes have attracted considerable attention because of their fascinating physical properties and promising technological applications in ultrahigh density memory [1], energy-harvesting devices, and advanced sensors [2,3]. The interest in tubular nanostructures comes from the idea that exotic phenomena may emerge due to the effects of chirality (or rolling direction) and curvature [4,5]. On the other hand, the continuous development of ultrahigh density memory and the miniaturization of piezoelectric devices call for a decrease in the size of FE components with no loss of ferroelectricity. This has led to extensive experimental efforts toward the fabrication of ABO_3-type perovskite FE nanotubes via various chemical and physical methods [6–11] as well as theoretical investigation of their unusual physical properties [5,12–15].

Ferroelectricity in perovskite crystals is a collective phenomenon that involves a delicate balance between long-range Coulomb and short-range covalent interactions. Due to depolarization and surface effects, FE distortion in FE thin films usually degrades or even vanishes with decreasing size [16–18]. For $PbTiO_3$ thin films grown on $SrTiO_3$ substrates, FE distortion disappears when the thickness decreases below a critical thickness of two unit cells [17]. In contrast with thin films, free-standing ultrathin $PbTiO_3$ nanotubes folded from (100) nanosheets undergo spontaneous polarization, despite their sidewalls being thinner than the critical thickness of the thin films [5]. The presence of spontaneous polarization in these ultrathin nanotubes suggests that tube curvature plays a crucial role in the stability of FE distortion. However, the spontaneous polarization in the (100) $PbTiO_3$ nanotube is an order of magnitude weaker than that of its bulk counterpart, which limits device performance.

Due to structural asymmetry, the physical properties of perovskite nanotubes are also dependent on the rolling direction and cutting surface of the prototype nanosheets. The rolling direction of a nanotube, described by a chirality vector, usually gives rise to a variety of novel properties and functionalities. For example, a slight difference in rolling direction causes a shift from a metallic to a semiconducting state in carbon nanotubes [19]. An unusual noncollinear helimagnetism appears in iron nanotubes for two specific rolling directions [20]. Recently, first-principles calculations predicted that the most energetically favorable $SrTiO_3$ single-wall nanotubes are folded from (110) $SrTiO_3$ nanosheets with a specific rolling direction of (m, 0) [4], indicating that the stability of perovskite nanotubes is chirality dependent. At room temperature, $SrTiO_3$ has a cubic structure without spontaneous polarization. Nevertheless, $SrTiO_3$ is an incipient FE and has the same crystalline structure as paraelectric $PbTiO_3$. Therefore, the stability of FE $PbTiO_3$ single-wall nanotubes (PTO-SWNTs) should depend on the rolling direction. In particular, FE $PbTiO_3$ has different physical properties from dielectric $SrTiO_3$, so the rolling direction may lead to unusual FE distortion in PTO-SWNTs folded from (110) nanosheets.

This paper investigates from first principles the energetic, structural, and FE properties of FE PTO-SWNTs folded from (110) nanosheets with different rolling directions. Based on density functional theory (DFT) calculations, we demonstrate that a remarkable spontaneous polarization, comparable to the bulk value, can stably exist in (110) PTO-SWNTs with a specific rolling direction of (m, 0). Furthermore, the chirality-dependent spontaneous polarization in PTO-SWNTs is shown to involve an intriguing interplay of couplings among antiferrodistortive (AFD), FE, and strain degrees of freedom.

II. SIMULATION METHOD AND MODELS

Calculations based on DFT were performed using the VASP program code [21]. Within the local density

*Corresponding author: jw@zju.edu.cn

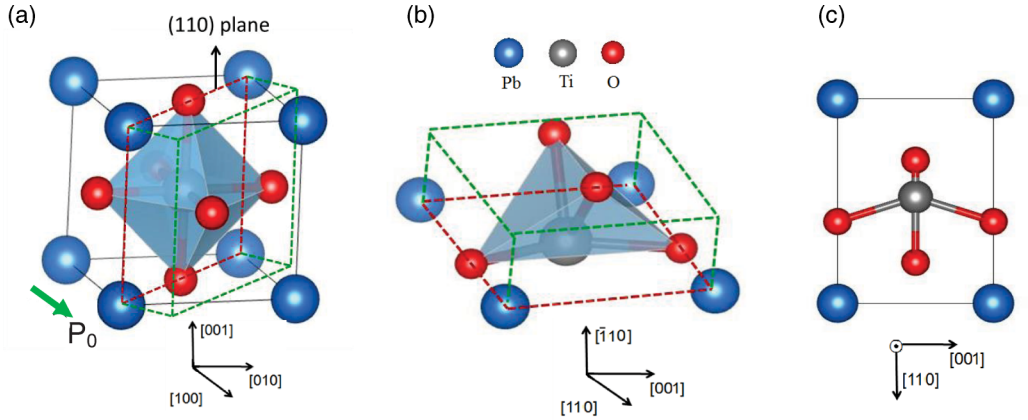

FIG. 1. (Color online) The primitive cell of stoichiometric nanosheet cut from $PbTiO_3$ bulk. (a) The cutting surface is a (110) plane in the tetragonal unit cell. (b) A primitive cell to form the nanosheets. (c) Projection of atoms of the primitive cell on ($\bar{1}10$) plane. The initial spontaneous polarization P_0 is along [100] direction in the tetragonal unit cell.

approximation, electron-ion interactions are described by projector-augmented wave potentials that explicitly include the valence electrons of 5d, 6s, and 6p for Pb; 3s, 3p, 3d, and 4s for Ti; and 2s and 2p for O [22,23]. The electronic wavefunctions are expanded in plane waves up to a cut-off energy of 500 eV. The conjugate-gradient algorithm is used in the present computational scheme to relax the ions until the force on each atom is less than 0.1 eV/nm [24]. Brillouin zone integration is sampled using a $1 \times 1 \times 6$ Monkhorst-Pack k-point mesh [25]. Within the supercell approach, a 20-Å-thick vacuum layer is introduced in the direction perpendicular to the tube axis in order to avoid undesirable interactions from neighboring tubes.

The nanotubes are modeled by rolling up stoichiometric nanosheets, which are obtained by cutting bulk $PbTiO_3$ along two parallel (110) planes. Figure 1 shows a schematic of the cutting surfaces in a prototype unit cell and the corresponding primitive cell for forming nanosheets, in which the initial spontaneous polarization is along the [100] direction. The relative displacements between oxygen and titanium ions in the [100] direction are decomposed into [110] and [$\bar{1}$10] directions, which give rise to equivalent polarization components in these two directions. The primitive cell includes only two atomic layers in the thickness direction ([$\bar{1}$10]), which is thinner than the FE critical thickness of the thin film [17]. Figure 2(a) shows the overall arrangement of atoms in the nanosheet formed by repeating the primitive cell shown in Fig. 1(c). In the present study, (110) PTO-SWNTs were constructed by rolling up the nanosheets in different directions. The rolling-up direction of the PTO-SWNTs is uniquely represented by the chiral vector $C_v = ma + nb \equiv (m,n)$, where **a** and **b** denote the primitive translation cell vectors of the tetragonal lattice, as shown in Fig. 2(a). In general, the nanotube can be folded in any arbitrary direction (m, n) for sheets with square or hexagonal 2D lattices. Due to the limitation of translational symmetry, only two rolling directions, (m, 0) and (0, n), are possible for the present rectangular lattice [26–28]. Therefore, we only consider nanotubes rolled in the (m, 0) and (0, n) directions, as shown in Fig. 2(b). According to the (110) cutting mode, Pb, Ti, and one O atom are present in one layer, whereas the other two O atoms exist in another layer. Depending on the choice of the outer layer, two differently terminated nanotubes are possible for each rolling direction: PbTiO-out and O-out nanotubes.

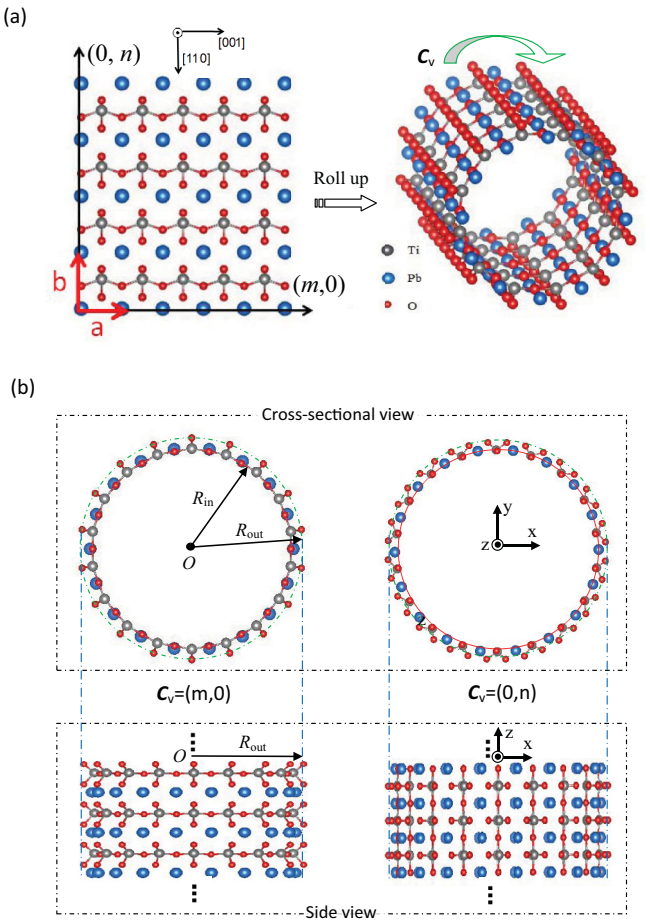

FIG. 2. (Color online) (a) The overall arrangement of atoms in the nanosheets formed by repeating the primitive cell of Fig. 1(c). The (110) $PbTiO_3$ single-wall nanotubes are constructed by rolling up the nanosheets with different chiralities. (b) The cross-sectional and side views of nanotubes with the chiralities of $\boldsymbol{C}_v = (m, 0)$ and $\boldsymbol{C}_v = (0, n)$.

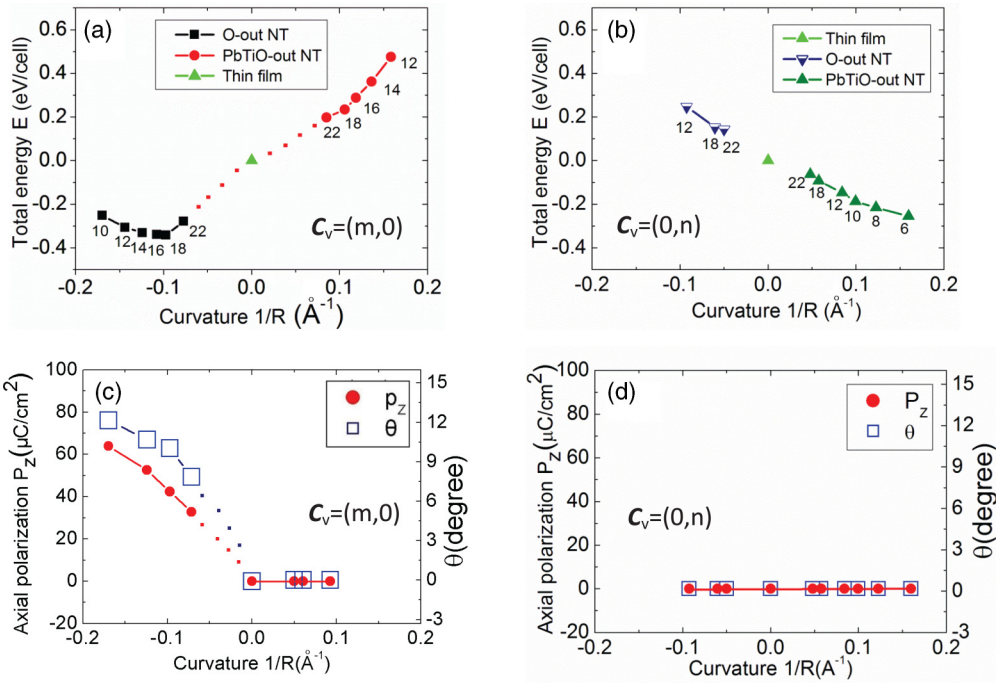

FIG. 3. (Color online) The curvature dependence of total energy in the PTO-SWNTs with different chiralities (a) $\boldsymbol{C}_v = (m, 0)$ and (b) $\boldsymbol{C}_v = (0, n)$. The curvature dependence of spontaneous polarization and titling angle of oxygen octahedra in the nanotubes with different chiralities, (c) $\boldsymbol{C}_v = (m, 0)$ and (d) $\boldsymbol{C}_v = (0, n)$. The total energy of PTO-SWNTs is at a minimum at $1/R = 0.097$ Å^{-1} ($m = 18$), where the polarization is 42.42 μC/cm^2.

III. RESULTS AND DISCUSSIONS

The structural asymmetry of the two sides of the nanosheet is the main driving force for the folding of nanosheets into nanotubes. The curvature of a nanotube plays an important role in the stability of its tubular structure [4,5]. To fully understand the effect of curvature on the stability of the PTO-SWNTs, we systematically investigated the energetic properties of nanotubes with a wide range of radii. Figure 3(a) shows the dependence of total energy on the curvature $1/R$ of the nanotubes with a rolling direction of $(m, 0)$, where the radius R is the average of the outer and inner radii, $R = (R_{out} + R_{in})/2$. The total energy of the flat thin film is set to zero as a reference state. Positive and negative curvatures correspond to PbTiO-out and O-out nanotubes, respectively. The curvature of the nanotubes induces a bending deformation in the tube wall, in which the outer shell experiences tension while the inner layer is under compression. For the PbTiO-out nanotubes, there are more atoms in the outer shell than in the inner one, so there is less chance for the atoms to move and reduce the deformation energy. As a result, the total energy for PbTiO-out nanotubes is higher than that for the thin films, suggesting that the PbTiO-out nanotubes are unstable. Furthermore, the total energy monotonically decreases with decreasing curvature for PbTiO-out PTO-SWNTs. Similar results were predicted for (110) $SrTiO_3$ SWNTs [4], suggesting that the present calculation method is reasonable for the tubular structures. When the curvature approaches zero, the total energy decreases to zero, and the nanotubes become flat thin films. In contrast, the total energy for O-out PTO-SWNTs is lower than that for the corresponding thin films, indicating that O-out PTO-SWNTs are more stable than the thin films. As the curvature of the O-out nanotubes increases from zero to 0.170 Å^{-1} ($m = 10$), the total energy first decreases and then increases. The lowest energy is located at $1/R = -0.097$ Å^{-1} ($m = 18$), at which the outer and inner radii are 22.70 Å and 18.46 Å, respectively. Interestingly, the curvature of the O-out (110) PTO-SWNT with the lowest energy is the same as that of the PbO-out (100) PTO-SWNTs, even though they have different symmetries [5]. However, the minimum total energy (−0.343 eV/cell) for the (110) PTO-SWNTs is much lower than that (−0.082 eV/cell) for the (100) PTO-SWNTs. This result implies that PTO-SWNTs rolled from (110) nanosheets are more stable than those rolled from (100) nanosheets.

PTO-SWNTs with different rolling directions have completely different atomic configurations, as shown in Fig. 2(b), which alters the curvature dependence of energy in the nanotubes. Figure 3(b) shows the curvature dependence of the total energy for PTO-SWNTs with a rolling direction of $(0, n)$. Interestingly, the overall trend of energy variation with curvature is the opposite of that for $(m, 0)$ nanotubes. The total energy for PbTiO-out nanotubes is lower than that for the thin film, while that of O-out nanotubes is higher than that for the thin film. This indicates that the former is more stable than the latter. Furthermore, the total energy changes monotonically with curvature for both O-out and PbTiO-out nanotubes, which is different to the case for $(m, 0)$ tubes. The chirality-dependent energetic properties are related to different deformations of oxygen octahedra in nanotubes with different rolling directions. Cutting along the (110) direction, oxygen octahedra are split into two parts, and only one-half remains in the nanotube [see the dark triangles in Fig. 2(b)]. Four Ti-O bonds are present in the remaining half. In $(0, n)$

nanotubes, the [110] direction of the primitive cell becomes the circumferential direction of the tube. As a result, two Ti-O bonds remain in the cross-sectional plane, as shown in Fig. 2(b). In O-out nanotubes, the two Ti-O bonds and half of the oxygen octahedra experience tension in the circumferential direction. The Ti-O bonds are covalent and often have a higher energy than Pb-O bonds when they are subjected to tension [29]. As a result, a higher energy is obtained for the O-out nanotubes; however, unlike for O-out nanotubes, Pb-O bonds are subjected to tension in PbTiO-out PTO-SWNTs, resulting in a lower energy due to the low covalency. Although the chirality is different, the energetic behavior of $(m, 0)$ nanotubes is also dependent on the deformation of Ti-O bonds and oxygen octahedra. For both rolling directions, tension in the Ti-O bonds or oxygen octahedra is responsible for the high energy for the PTO-SWNTs. Therefore, PTO-SWNTs are energetically favorable when there is no tension in the oxygen octahedra.

The effect of the rolling direction on the ferroelectricity of PTO-SWNTs with different curvatures was investigated by measuring the spontaneous polarization. The polarization is calculated based on the Berry phase theory [30]. The calculated spontaneous polarizations for PTO-SWNTs with different curvatures and rolling directions are given in Figs. 3(c) and 3(d). It was found that spontaneous polarizations exist only in nanotubes with a rolling direction of $(m, 0)$. When the nanosheets are rolled up into $(m, 0)$ nanotubes, the initial polarization vector gives rise to two equivalent components in the radial and axial directions. After relaxation, the radial polarization disappears for both PbTiO-out and O-out nanotubes. Note that the wall thickness of the nanotubes is only 2.092 Å, so it is reasonable that FE distortion is completely suppressed in the radial direction by the depolarization field. Surprisingly, a remarkable axial polarization exists for the O-out nanotubes, even though the tube wall is much thinner than the FE critical thickness of the flat thin film. The existence of this axial polarization indicates the absence of a FE critical thickness in (110) $PbTiO_3$ nanotubes, which was also the case in (100) $PbTiO_3$ nanotubes [5]. The axial polarization for (110) PTO-SWNTs with a curvature of -0.097 Å^{-1} $(m = 18)$ was calculated to be 42.42 μC/cm^2, which is comparable to the bulk value of 78.6 μC/cm^2 and one order of magnitude higher than that for (100) PTO-SWNTs. Due to the unusual geometry, the barrier for axial polarization switching in the nanotubes could be significantly different from that in bulk PTO. The energy barrier for polarization switching in the nanotube is calculated to be 70 (meV/cell), which is larger than the value of 56 (meV/cell) in bulk PTO, which means polarization switching is harder in the nanotube than in bulk PTO.

The polarization in (110) nanotubes stems from breaking the symmetry of oxygen octahedra along the axial direction due to the asymmetric cutting of the prototype unit cell. This symmetry breaking results in a large tilt of oxygen octahedra in the longitudinal section of the nanotubes, which is indicated by the angle θ in Fig. 4(a). Due to this tilting, the projection of the oxygen atoms on the tube wall also changes after relaxation. The distances between the projected oxygen and Ti atoms become longer and shorter in the upper and lower parts of the dotted rectangle, respectively, as shown in Fig. 4(c). For

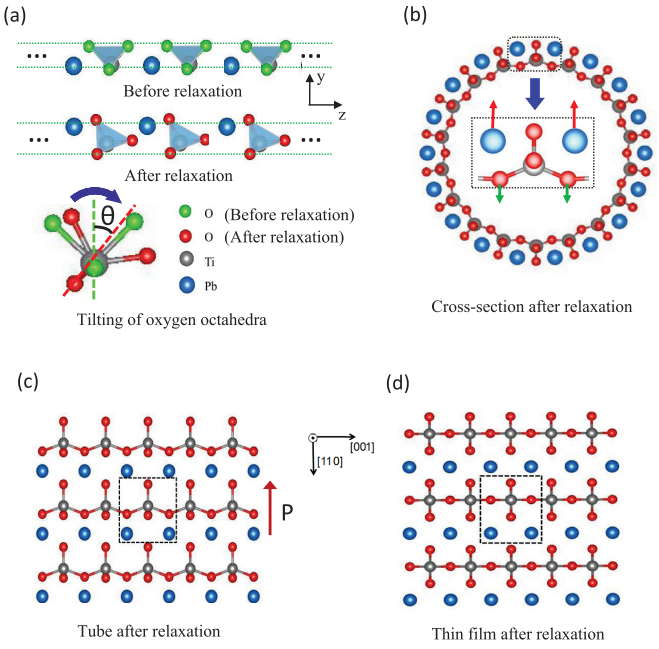

FIG. 4. (Color online) The detailed atomic configuration after relaxation for the O-outside nanotube with the lowest energy ($m = 18$). (a) Tilting of oxygen octahedra in the longitudinal section after relaxation. (b), (c) Cross-sectional and expanded side views of the nanotube after relaxation, respectively. (d) Side view of thin film after relaxation.

comparison, the atomic projection of a relaxed thin film is also shown in Fig. 4(d), in which the atoms form a paraelectric structure with a higher symmetry. There is no titling of oxygen octahedra in the thin film, implying that the titling of oxygen octahedra, a type of AFD distortion, is coupled with the FE distortion in the PTO-SWNTs. The curvature dependence of the polarization and titling angle in Figs. 3(c) and 3(d) clearly demonstrates the strong coupling between FE distortion and AFD distortion. The FE-AFD coupling is responsible for the stability of the FE distortion in the nanotube, which gives rise to improper ferroelectricity in the (110) $PbTiO_3$ nanotubes. A similar improper ferroelectricity was also found in perovskite oxide artificial superlattices, where the interfacial strain plays a critical role in the FE-AFD coupling [31,32]. In the present (110) $PbTiO_3$ nanotubes, various strain states are associated with different chiralities and curvatures, which leads to the appearance of chiral selectivity of improper ferroelectricity.

Strain originating from curvature has a strong influence on the magnitude of polarization in (110) $PbTiO_3$ nanotubes. The magnitude of the axial polarization increases when the curvature increases, as shown in Fig. 3(c). At the same time, the total energy also increases with curvature when the energy is above the minimum energy. The increase in total energy is due to an increase in strain with curvature. Therefore, the nanotubes become unstable when the polarization increases past the point of minimum energy. When comparing Fig. 3(c) with 3(a), it can be seen that the PTO-SWNTs can be stable at the minimum energy point, where the polarization is still large. It is important to note that the minimum energy for the nanotube is much lower than that for the flat thin film, i.e.,

the so-called strain energy is negative, indicating that PTO-SWNTs with a large polarization can be spontaneously folded from nanosheets. The appearance of the large polarization in PTO-SWNTs with negative strain energy holds promise for a wide range of applications such as ultrahigh density random access memory and nanoscale energy harvesting devices.

On the other hand, strain also plays a decisive role in the titling of oxygen octahedra in PTO-SWNTs. When the nanosheets are folded into O-out nanotubes, the inner PbTiO shell is under compression. To release this compressive stress, a Pb atom and two oxygen atoms move outwards and inwards, respectively, along the radial direction, as shown in Fig. 4(b). The movement of atoms is a steric phenomenon, in which the large Pb atoms are relocated at periodic intervals along the outer shell. As a result, tilting of the oxygen octahedra is induced in the axial direction by the movement of Pb and O atoms in the radial direction. This is the origin of the large polarization in the nanotubes, which involves interplay of couplings among AFD, FE, and strain degrees of freedom. In addition, titling of oxygen octahedra takes place in the longitudinal section of the tube wall, which is completely different from the rotation of oxygen octahedra in the cross section of the (100) $PbTiO_3$ nanotube [5]. This titling leads to large displacements of oxygen atoms in the axial direction of the nanotubes, which enhances the polarization in this direction.

To check the stability of FE distortion in short nanotubes, we perform the calculations of a short nanotube with one unit cell separated by vacuum in the axial direction. It is found that AFD atomic displacements still exist in the short nanotube. The deviation in the axial direction between O atoms and Ti atoms in the middle layer of unit cell is 0.653 Å, which is close to the value of 0.680 Å in the infinite long nanotube, indicating that the FE distortion is stable in the short nanotube although there is a depolarizing field.

IV. CONCLUSION

In summary, we have demonstrated that a remarkable FE distortion, comparable to the bulk value, can stably exist in PTO-SWNTs with a specific chirality of $(m, 0)$, whereas the FE phase is absent from nanotubes with other chiralities and from the unfolded thin films. The chirality-dependent polarization originates from tilting of oxygen octahedra, which gives rise to improper ferroelectricity. Strains originating from different curvatures and chiralities play unique roles in the stabilization of the single-wall tubular structure and the strong coupling between FE and AFD distortions. The PTO-SWNTs with large polarization not only exhibit fascinating coupling properties but also hold promise for technological applications. The present results may stimulate new experimental investigations of single-wall perovskite nanotubes as FE components in addition to theoretical studies of the interplay of couplings among AFD, FE, and strain degrees of freedom.

ACKNOWLEDGMENTS

This work was financially supported by Grants-in-Aid for Scientific Research (No. 21226005 and No. 25000012) and a Research Fellowship (No. P12058) from the Japan Society for the Promotion of Science, the Nature Science Foundation of China (No. 11002123, No. 11090333, and No. 11321202), Zhejiang Provincial Natural Science Foundation (No. R6110115), and the research Fund from China Academy of Engineering Physics (No. 2013KJZ02 and No. 2013B0302044). Computations were performed in National Supercomputer Center in Tianjing, China.

[1] W. Lee, H. Han, A. Lotnyk, M. A. Schubert, S. Senz, M. Alexe, D. Hesse, S. Baik, and U. Gösele, Nat. Nanotechnol. **3**, 402 (2008).
[2] W. Wu, S. Bai, M. Yuan, Y. Qin, Z. L. Wang, and T. Jing, ACS Nano **6**, 6231 (2012).
[3] J. Scott, Science **315**, 954 (2007).
[4] S. Piskunov and E. J. Spohr, Phys. Chem. Lett. **2**, 2566 (2011).
[5] T. Shimada, X. Wang, Y. Kondo, and T. Kitamura, Phys. Rev. Lett. **108**, 067601 (2012).
[6] Y. Luo, I. Szafraniak, V. Nagarjan, R. Wehrspohn, M. Steinhart, J. H. Wendorff, N. D. Zakharov, R. Ramesh, and A. Alexe, Appl. Phys. Lett. **83**, 440 (2003).
[7] B. A. Hernandez, K. S. Chang, and E. R. Fisher, Chem. Mater. **14**, 481 (2002).
[8] F. D. Morrison, Y. Luo, I. Szafraniak, V. Nagarajan, R. B. Wehrspohn, M. Steinhart, J. H. Wendorff, N. D. Zakharov, E. D. Mishina, K. A. Vorotilov, A. S. Sigov, S. Nakabayashi, M. Alexe, R. Ramesh, and J. F. Scott, Rev. Adv. Mater. Sci. **4**, 114 (2003).
[9] P. M. Rørvik, T. Grande, and M. A. Einarsrud, Adv. Mater. **23**, 4007 (2011).
[10] A. Bernal, A. Tselev, S. Kalinin, and N. Bassiri-Gharb, Adv. Mater. **24**, 1160 (2012).
[11] J. Kim, S. A. Yang, Y. C. Choi, J. K. Han, K. O. Jeong, Y. J. Yun, J. Kim, S. M. Yang, D. Yoon, H. Cheong, K. S. Chang, T. W. Noh, and S. D. Bu, Nano Lett. **8**, 1813 (2008).
[12] A. N. Morozovska, M. D. Glinchuk, and E. A. Eliseev, Phase Transitions **80**, 71 (2007).
[13] J. Wang and M. Kamlah, Phys. Rev. B **80**, 012101 (2009).
[14] Y. Zheng, C. H. Woo, and B. Wang, J. Phys.: Condens. Matter. **20**, 135216 (2008).
[15] J. Wang and M. Kamlah, Appl. Phys. Lett. **93**, 042906 (2008).
[16] R. Kretschmer and K. Binder, Phys. Rev. B **20**, 1065 (1979).
[17] D. D. Fong, G. B. Stephenson, S. K. Streiffer, J. A. Eastman, O. Auciello, P. H. Fuoss, and C. Thompson, Science **304**, 1650 (2004).
[18] J. Junquera and P. Ghosez, Nature **422**, 506 (2003).
[19] J. W. G. Wildoer, L. C. Venema, A. G. Rinzler, R. E. Smalley, and C. Dekker, Nature **391**, 59 (1998).
[20] T. Shimada, J. Okuno, and T. Kitamura, Nano Lett. **13**, 2792 (2013).
[21] G. Kresse and J. Furthmüller, Comput. Mater. Sci. **6**, 15 (1996).

[22] N. Troullier and J. L. Martins, Phys. Rev. B **43**, 1993 (1991).
[23] P. E. Bloch, Phys. Rev. B **50**, 17953 (1994).
[24] F. Shimojo, Y. Zempo, K. Hoshino, and M. Watabe, Phys. Rev. B **52**, 9320 (1995).
[25] M. J. Monkhorst and J. D. Pack, Phys. Rev. B **13**, 5188 (1976).
[26] A. N. Enyashin and G. Seifert, Phys. Status Solidi B **242**, 1361 (2005).
[27] L. Chernozatonskii, P. Sorokin, and A. Fedorov, Phys. Solid State **48**, 2021 (2006).
[28] R. A. Evarestov, A. B. Bandura, M. V. Losev, S. Piskunov, and Yu. F. Zhukovskii, Phys. E **43**, 266 (2010).
[29] S. de Lazaro, E. Longo, J. R. Sambrano, and A. Beltran, Surf. Sci. **552**, 149 (2004).
[30] R. Resta, J. Phys.: Condens. Matter. **12**, R107 (2000).
[31] P. Aguado-Puente, P. García-Fernández, and J. Junquera, Phys. Rev. Lett. **107**, 217601 (2011)
[32] E. Bousquet, M. Dawber, N. Stucki, C. Lichtensteiger, P. Hermet, S. Gariglio, J. M. Triscone, and P. Ghosez, Nature **452**, 732 (2008).